J. Phys. B: At. Mol. Opt. Phys. **30** (1997) L719–L725. Printed in the UK PII: S0953-4075(97)86128-7

LETTER TO THE EDITOR

On the generation of ultra-broad bandwidth light in air at atmospheric pressure

G S McDonald†§, G H C New†, L L Losev‡ and A P Lutsenko‡

† Laser Optics and Spectroscopy Group, The Blackett Laboratory, Imperial College of Science, Technology and Medicine, Prince Consort Road, London SW7 2BZ, UK

‡ P N Lebedev Physical Institute, Leninsky Prospekt 53, 117924 Moscow, Russia

Received 21 July 1997, in final form 5 September 1997

Abstract. We predict that ultra-broadband light consisting of over 150 distinct frequencies of comparable energy can be generated in air at atmospheric pressure by stimulated Raman scattering using resonant symmetric pumping. Nanosecond input pulses and the highest available intensities are found to be optimal. Gain suppression analysis, incorporating a finite Stokes shift, gives a qualitative explanation of the pumping requirements.

Non-parametric stimulated Raman scattering is well established as a simple and efficient method of converting laser radiation to one or more lower (Stokes) frequencies. However, parametric Raman conversion to higher frequencies, or the simultaneous generation of multiple Raman lines, has generally been found to be much less efficient. The common assumption has been that, for efficient frequency conversion, phase-matching conditions dictate the angular geometry of higher-order waves. More recently, with H_2 gas as the Raman medium, we have shown that the collinear generation of higher orders using two input beams, with a frequency difference which is resonant with the Raman transition and which are temporally symmetric (of matching intensity, shape and linear polarization), permits a maximum interaction volume and has much greater potential for the generation of ultra-broadband light (Losev and Lutsenko 1993, 1996, McDonald *et al* 1994, 1995, McDonald 1995).

The use of air as the nonlinear medium has obvious attractions. Experiments demonstrating multifrequency generation using the rotational transitions of N_2 have been performed, but the configurations used were highly non-optimal for bandwidth production. In Eimerl *et al* (1993), only around 15 sidebands were generated because a single pump beam was employed; new frequencies had to grow from background noise—a relatively inefficient process involving cascade down-conversion from a number of distinct rotational transitions. Dangor *et al* (1989) investigated the propagation of two light beams in air at atmospheric pressure and rotational Raman scattering was observed to be the dominant effect. Their configuration generated several sidebands even though the frequency difference of their input beams was 10 linewidths away from resonance.

In this letter, we consider the resonant symmetric pumping of a single rotational transition of atmospheric N_2, the $J = 8 \rightarrow 10$ transition which defines a Stokes shift

§ E-mail address: g.mcdonald@ic.ac.uk

0953-4075/97/210719+07$19.50

of 76 cm^{-1} (Losev and Lutsenko 1994), and predict that a single beam containing over 150 lines of comparable energy may be generated. A wealth of applications for these results is possible, including frequency conversion, atmospheric transmission of optical energy and information, visual displays, sensing, measurement techniques, spectroscopy and inertial confinement fusion (Eimerl *et al* 1992, McDonald *et al* 1995).

To model ultra-broadband multifrequency Raman generation (UMRG), the electric field is expanded in terms of plane waves whose frequencies are given by $\omega_n = \omega_0 + n\omega_R$ ($n = 0, \pm1, \pm2, \ldots$) where ω_0 and ω_R are the pump and Stokes frequency, respectively. The dimensionless equations for the propagation, in z, of the nth normalized electric field envelope, A_n, and the dynamics of the polarization wave, P, are (Losev and Lutsenko 1993, McDonald *et al* 1994)

$$\frac{\partial A_n}{\partial Z} = \frac{\omega_n}{2\omega_0}[P^* A_{n+1}\exp(-i\gamma_{n+1}Z) - P A_{n-1}\exp(i\gamma_n Z)] \tag{1}$$

$$\left(\frac{T_2}{t_p}\right)\frac{\partial P}{\partial \tau} = -P + \sum_j A_j A_{j-1}^* \exp(-i\gamma_j Z) \tag{2}$$

where $Z = gI_0 z$, $g = 0.005$ cm GW^{-1} is the measured Raman gain coefficient for air at 1 atmosphere pressure and at a temperature of 290 K (Rokni and Flusberg 1986), I_0 is the input intensity, τ is local time (in units of input pulse width t_p) and $T_2 = 130$ ps is the dephasing time. Dispersion defines a set of normalized mistunings, γ_n, which are determined by the value of γ_1 together with a dispersion law. Assuming a Cauchy formula for the frequency dependence of the refractive index, μ_n, one finds that $\gamma_n = n\gamma_1(1 + (n-1)/2B_0)$ where $\gamma_1 = (k_1 + k_{-1} - 2k_0)/gI_0$, $k_n = \mu_n\omega_n/c$ and $B_0 = \omega_0/\omega_R$. Since this work deals with atmospheric Raman generation, as opposed to UMRG in pure N_2, we use the dispersion law for air. We consider resonant and symmetric pumps (square pulses of equal amplitude, parallel polarization and separated in frequency by 76 cm^{-1}) supplied by a Nd:YAG laser, $\omega_0/2\pi c = 18\,900$ cm^{-1}, and sideband (Losev and Lutsenko 1994). All other fields are initially zero. In our previous work (McDonald *et al* 1994, 1995, McDonald 1995), we investigated UMRG in H_2 using input pulses of square, Gaussian and noisy character. While the duration and energy of the pump pulses were found to be important parameters, the bandwidth and energy spectra generated were found to be remarkably insensitive to the particular choice of input pulse shape (provided that the pumping remained symmetric). We have verified that the results presented here are also insensitive to the details of the pump pulse shapes.

Our analyses of dispersionless UMRG predict that, under CW conditions, a bandwidth of $B \approx B_0 = \omega_0/\omega_R$ is possible (Losev and Lutsenko 1993) and that, in the highly transient regime, this figure may be enhanced by around 40% (Losev and Lutsenko 1996). However, numerical simulations have shown that background dispersion plays a critical role in determining the generated bandwidth (McDonald *et al* 1994, 1995, McDonald 1995). In physical terms, the absence of dispersion ($\gamma_1 = 0$) implies exact phase-matching and this maximizes the amount of gain suppression (Shen and Bloembergen 1965). A rapid exhaustion of the polarization wave results which, in turn, halts bandwidth production after a certain distance. On the other hand, there is no gain suppression for high dispersion ($\gamma_1 \gg 1$) but the parametric processes, which are necessary for bandwidth production, are suppressed. Between the two limits, of maximum and zero gain suppression, there exists an optimal level of suppression which leads to a maximum in the generated bandwidth. In the case of H_2 gas, such optimization is predicted to permit a bandwidth of $B \approx 1.5B_0$ (McDonald *et al* 1994, 1995, McDonald 1995). Since gain suppression is parametrized by

the normalized dispersion variable γ_1 (Shen and Bloembergen 1965), this maximum in the bandwidth can be associated with an optimum level of dispersion, $\gamma_1 = \gamma_1^{\text{opt}}$.

To determine the role of background dispersion for UMRG in air, equations (1) and (2) have been solved numerically. The time domain of each wave was discretized into 500 complex points and up to 800 such waves were simulated. We shall only present results for propagation distances of up to 20 m. This is because our model equations apply to a (locally) planar section of the propagating fields and we expect that complicated transverse effects may occur around this distance. To justify the assumption of plane-wave interactions, one needs to consider beams which are sufficiently broad that significant diffractive reshaping does not occur. However, since we deal with beams which have a specific peak intensity, a broader beam implies a higher input power and other effects, such as self-focusing, may become important. In fact, our preliminary studies of finite beam effects suggest that it is actually the UMRG process which, in combination with beam diffraction and a finite transverse intensity curvature of the fields, gives rise to the ultimate limitation on the distance over which plane-wave modelling can be used.

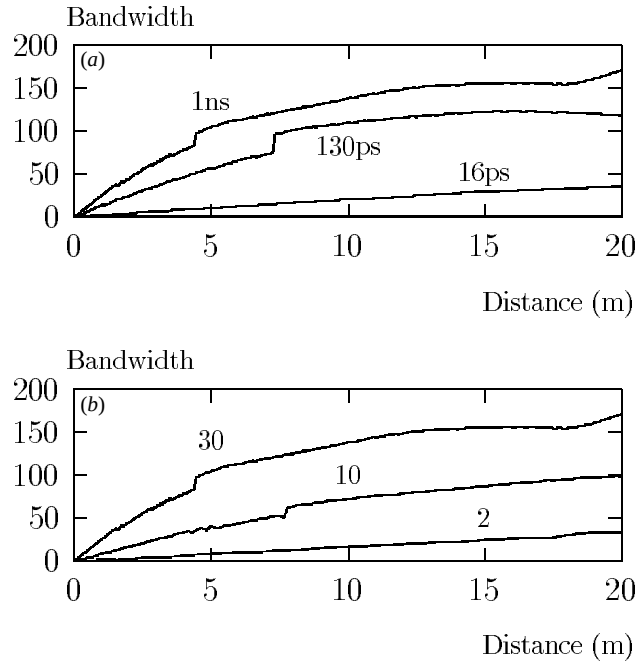

Figure 1. Number of frequencies of comparable energy (bandwidth) generated during atmospheric propagation. (*a*) $I_0 = 30$ GW cm^{-2}. Curves are labelled with the input pulse width. (*b*) $t_p = 1$ ns. Curves are labelled with input intensities (in GW cm^{-2}).

Graphs showing the increase in bandwidth with propagation distance for three different pulse widths ($t_p/T_2 = 8, 1$ and $\frac{1}{8}$) are presented in figure 1(*a*). The results clearly show that the input pulse width can play an important role and that the bandwidth is generally lower for shorter pulses. We find that a pulse width of about an order of magnitude longer than T_2 is optimal and that, in this case, the bandwidth closely follows that predicted by the corresponding CW simulation. The step-like features, which are quite evident in the 1 ns and 130 ps curves, are a common feature in UMRG. We have found that prior to these steps the UMRG process is approximately described by the $\gamma_1 = 0$ solution. In this regime,

parametric processes dominate and the spectrum generated is composed of roughly equal proportions of Stokes and anti-Stokes waves. In the vicinity of these step features, non-parametric (down-conversion) processes begin to make a large contribution to the frequency conversion. This gives rise to a relatively sudden growth of additional Stokes waves, which results in a sharp increase in bandwidth (arising from the extension of the low-frequency section of the UMRG spectrum).

Figure 1(*b*) displays the role of input intensity for $t_p/T_2 = 8$. In contrast to UMRG in H_2, we find that the highest available input intensities are optimal. Surprisingly, dispersion does not, in these cases, give rise to bandwidth enhancement above the theoretical prediction for dispersionless CW UMRG of $B_0 \approx 250$. We have limited the results to $I_0 \leqslant 30$ GW cm^{-2} to avoid gas breakdown, but find that higher I_0 and z does lead to the predicted bandwidth enhancement.

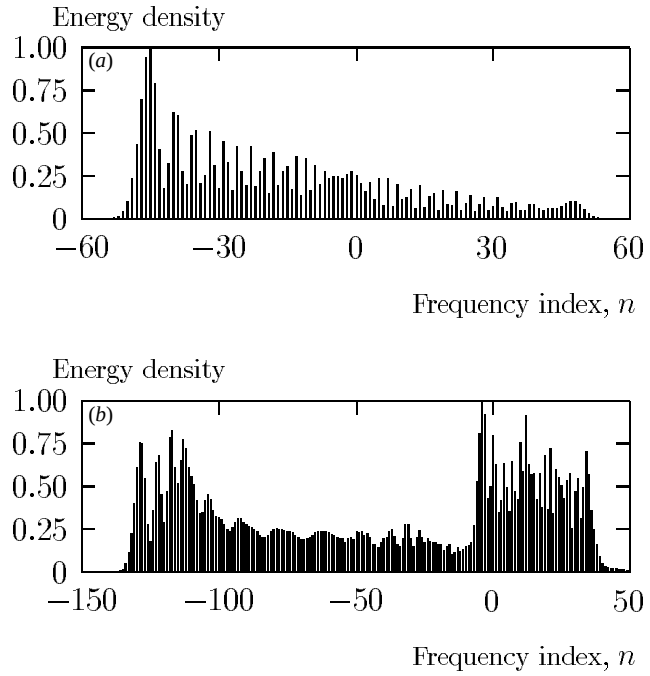

Figure 2. Output spectra (time-integrated intensity profiles) generated after (*a*) a short air path of 4.5 m and (*b*) a long air path of 20 m. The units are defined so that the peak energy density is normalized to unity. Parameters are $t_p = 1$ ns and $I_0 = 30$ GW cm^{-2}.

Figures 2(*a*) and (*b*) show typical energy spectra of the beam after short ($z = 4.5$ m) and long ($z = 20$ m) air paths, respectively. It should be stressed that other techniques for generating multifrequency beams generally result in only a few lines, or broadband spectra that need to be presented on a logarithmic scale. However, a remarkable characteristic of beams generated in this way is that each new frequency channel carries approximately an equal share of the propagating energy and the resulting spectra can be presented on a linear scale. Figure 2(*a*) demonstrates that over 100 components are generated after only 4.5 m. The efficiency of bandwidth generation is such that many competing nonlinear processes will be greatly suppressed (Eimerl *et al* 1992, 1993). While each line in the spectrum continues to contribute to the polarization wave which drives the multifrequency interactions, the rapid re-distribution of energy means that the intensity at any one frequency (which could

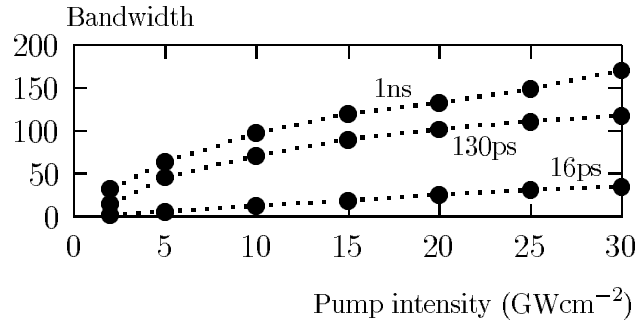

Figure 3. Bandwidth of the multifrequency beam at a distance of $z = 20$ m. Curves are labelled with the input pulse width.

act as a pump for a spontaneous, and non-resonant, competing process) is quickly depleted by orders of magnitude. Figure 3 gives a summary of the predictions at a fixed distance; underlining the trends discussed above and demonstrating continuity between the different parameter regimes.

In studies of UMRG using H_2, $\gamma_1^{\rm opt} \approx 2 \times 10^{-3}$ was found (McDonald *et al* 1994). For air, $I_0 = 30$ GW cm^{-2} implies $\gamma_1 \approx 0.45 \times 10^{-3}$ and simulations reveal that $\gamma_1^{\rm opt} \approx 0.025 \times 10^{-3}$ for $B \approx 1.5B_0$ at $z \approx 150$ m. To gain a qualitative insight into the reason why $\gamma_1^{\rm opt}$ can vary by two orders of magnitude between different media, we have generalized the classic gain suppression analysis of Shen and Bloembergen (1965) to include a finite Stokes shift. In this letter, we give a brief outline of this analysis and defer a more complete description to a future publication.

Parametric processes in UMRG generate *pairs* of new frequencies in which each wave of the pair is out of phase with the other. This phase relationship gives rise to contributions to the polarization wave which cancel each other and the medium grating eventually becomes exhausted. The symmetry of such parametric generation, and the accompanying polarization depletion, effectively suppresses the Raman gain. To analyse this effect, it is necessary to consider a subsystem of the CW UMRG equations and the parametric generation of a *pair* of waves, A_{n-1} and A_{n+1}. Our objective is to quantify the gain experienced by these waves and, for this purpose, we consider that the intermediate wave, A_n, is equal to unity and that other waves are negligible. We seek eigenfunctions of the resulting subsystem of the form

$$A_{n-1}(Z) = a_{n-1} \exp\left[\left(K + \tfrac{1}{2}{\rm i}(\gamma_{n+1} - \gamma_n)\right)Z\right] \tag{3}$$

$$A_{n+1}^*(Z) = a_{n+1}^* \exp\left[\left(K - \tfrac{1}{2}{\rm i}(\gamma_{n+1} - \gamma_n)\right)Z\right] \tag{4}$$

where a_{n-1} and a_{n+1}^* are complex amplitudes and the gain per unit Z, g^+, is given by the real part of K. Substitution of (3) and (4) into the propagation equations for A_{n-1} and A_{n+1}^* yields the following (complex) quadratic equation for K:

$$K^2 + \epsilon K + \tfrac{1}{2}{\rm i}(n+1)(\gamma_{n+1} - \gamma_n) + \tfrac{1}{4}(\gamma_{n+1} - \gamma_n)^2 = 0 \tag{5}$$

where $\epsilon = 1/B_0 = \omega_{\rm R}/\omega_0$. To facilitate a direct comparison with the results of Shen and Bloembergen (1965), we consider here the case of equations (3)–(5) with $n = 0$. Solving for the dimensionless gain, we then find that

$$g^+ = -\frac{\epsilon}{2} + \frac{1}{2\sqrt{2}}\left[\epsilon^2 - \gamma_1^2 + \sqrt{\left(\epsilon^2 - \gamma_1^2\right)^2 + 4\gamma_1^2}\,\right]^{1/2}. \tag{6}$$

The corresponding result of Shen and Bloembergen (1965), which applies in the limit of zero Stokes shift, can be recovered from (6) by setting $\epsilon = 0$.

Since $\epsilon \approx 3.1 \times 10^{-2}$ for the S(1) transition of H_2 and $\epsilon \approx 4.0 \times 10^{-3}$ for air, we find that to obtain the same gain, g^+, and hence the same degree of gain suppression, the respective values of γ_1^{opt} are smaller by one or two orders of magnitude. Thus, it is clear from (6) that the inclusion of a finite Stokes shift is necessary for an accurate description of the gain suppression in these cases. In other words, we find that the optimization of UMRG bandwidth is parametrized by *both* γ_1 and ϵ. In figure 4, we plot the normalized gain curves for air and H_2 in the vicinity of γ_1^{opt}. A key feature is that $g^+ \to 0$ as $\gamma_1 \to 0$, even when finite Stokes shift is accounted for. Thus, we can report that gain suppression is still maximized, and is in fact complete, in the zero dispersion limit.

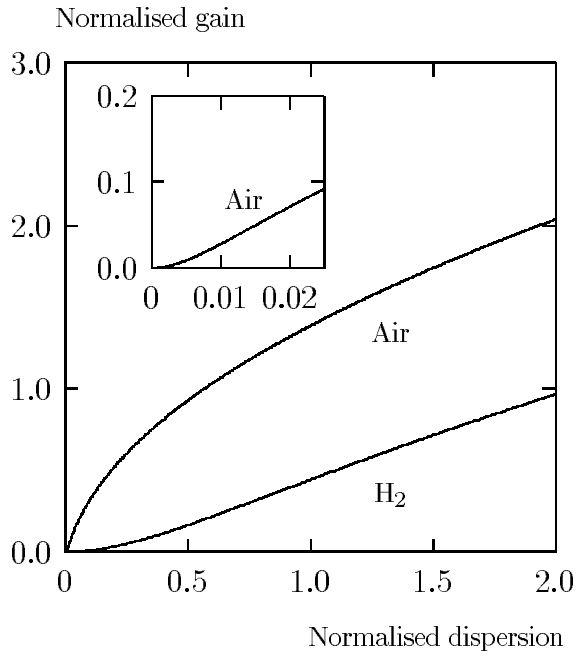

Figure 4. Normalized gain (g^+ in units of 10^{-2}) as a function of normalized dispersion (γ_1 in units of 10^{-3}) in air and H_2. Inset: detail of the gain in air for low γ_1.

In addition to significantly different quantitative estimates of the normalized gain, it can be seen that finite ϵ also introduces new qualitative features into the gain curves. Each curve is composed of different regimes defined by the relative values of γ_1 and ϵ. For example, when $\gamma_1^2 \ll \epsilon^4/4$ each curve behaves as $\gamma_1^2/4\epsilon^3$, whereas for $\epsilon^4/4 \ll \gamma_1^2 \ll \epsilon^2$ the curvature has the opposite sign and $g^+ \approx -\epsilon/2 + \sqrt{\gamma_1}/2$. Each of the above values of γ_1^{opt} is found to be in the lower γ_1 region of this latter regime. It is important to note that the smaller Stokes shift in air reduces greatly the amount of gain suppression for fixed γ_1. Thus, to attain the same optimal level of gain suppression, γ_1 must also be reduced. While this relatively simple analysis cannot fully account for the complexity of UMRG, as illustrated in figure 2 for example, we believe that the new qualitative features uncovered by this analysis are a clear indication of the physical character of the processes involved in optimizing UMRG.

We thank Dr M J Shaw for many useful discussions. This research was supported in part by UK EPSRC grant GR/K 54748 and INTAS grant 93-1103.

References

Dangor A E *et al* 1989 *J. Phys. B: At. Mol. Opt. Phys.* **22** 797
Eimerl D, Kruer W L and Campbell E M 1992 *Comment. Plasma Phys.* **15** 85
Eimerl D, Milam D and Yu J 1993 *Phys. Rev. Lett.* **70** 2738
Losev L L and Lutsenko A P 1993 *Kvantovaya Electron. (Moscow)* **20** 1054
——1994 *Kvantovaya Electron. (Moscow)* **21** 965
——1996 *Opt. Commun.* **132** 489
McDonald G S 1995 *Opt. Lett.* **20** 822
McDonald G S, New G H C, Losev L L, Lutsenko A P and Shaw M J 1994 *Opt. Lett.* **19** 1400
——1995 *Inst. Phys. Conf. Series* **140** 85
Rokni M and Flusberg A 1986 *IEEE J. Quantum Electron.* **QE-22** 1102
Shen Y R and Bloembergen N 1965 *Phys. Rev.* A **137** 1787